

Vibrational study of HgGa₂S₄ under high pressure

R. Vilaplana, M. Robledillo, O. Gomis, J. A. Sans, F. J. Manjón et al.

Citation: *J. Appl. Phys.* **113**, 093512 (2013); doi: 10.1063/1.4794096

View online: <http://dx.doi.org/10.1063/1.4794096>

View Table of Contents: <http://jap.aip.org/resource/1/JAPIAU/v113/i9>

Published by the [American Institute of Physics](#).

Related Articles

Liquid-phase deposition of thin Si films by ballistic electro-reduction
Appl. Phys. Lett. **102**, 022107 (2013)

Spiral growth of topological insulator Sb₂Te₃ nanoplates
Appl. Phys. Lett. **102**, 013105 (2013)

Stimulated crystallization of melt-quenched Ge₂Sb₂Te₅ films employing femtosecond laser double pulses
J. Appl. Phys. **112**, 123520 (2012)

Controlled joining of Ag nanoparticles with femtosecond laser radiation
J. Appl. Phys. **112**, 123519 (2012)

Structural, elastic, and vibrational properties of layered titanium dichalcogenides: A van der Waals density functional study
J. Chem. Phys. **137**, 224509 (2012)

Additional information on *J. Appl. Phys.*

Journal Homepage: <http://jap.aip.org/>

Journal Information: http://jap.aip.org/about/about_the_journal

Top downloads: http://jap.aip.org/features/most_downloaded

Information for Authors: <http://jap.aip.org/authors>

ADVERTISEMENT



AIP Advances

Now Indexed in
Thomson Reuters
Databases

Explore AIP's open access journal:

- Rapid publication
- Article-level metrics
- Post-publication rating and commenting

Vibrational study of HgGa_2S_4 under high pressure

R. Vilaplana,^{1,a)} M. Robledillo,¹ O. Gomis,¹ J. A. Sans,² F. J. Manjón,² E. Pérez-González,³ P. Rodríguez-Hernández,³ A. Muñoz,³ I. M. Tiginyanu,⁴ and V. V. Ursaki⁴

¹Centro de Tecnologías Físicas: Acústica, Materiales y Astrofísica, MALTA Consolider Team, Universitat Politècnica de València, 46022 València, Spain

²Instituto de Diseño para la Fabricación y Producción Automatizada, MALTA Consolider Team, Universitat Politècnica de València, 46022 València, Spain

³Departamento de Física Fundamental II, Instituto de Materiales y Nanotecnología, MALTA Consolider Team, Universidad de La Laguna, 38205 Tenerife, Spain

⁴Institute of Applied Physics, Academy of Sciences of Moldova, 2028 Chisinau, Moldova

(Received 8 December 2012; accepted 18 February 2013; published online 7 March 2013)

In this work, we report on high-pressure Raman scattering measurements in mercury digallium sulfide (HgGa_2S_4) with defect chalcopyrite structure that have been complemented with lattice dynamics *ab initio* calculations. Our measurements evidence that this semiconductor exhibits a pressure-induced phase transition from the completely ordered defect chalcopyrite structure to a partially disordered defect stannite structure above 18 GPa which is prior to the transition to the completely disordered rocksalt phase above 23 GPa. Furthermore, a completely disordered zincblende phase is observed below 5 GPa after decreasing pressure from 25 GPa. The disordered zincblende phase undergoes a reversible pressure-induced phase transition to the disordered rocksalt phase above 18 GPa. The sequence of phase transitions here reported for HgGa_2S_4 evidence the existence of an intermediate phase with partial cation-vacancy disorder between the ordered defect chalcopyrite and the disordered rocksalt phases and the irreversibility of the pressure-induced order-disorder processes occurring in ordered-vacancy compounds. The pressure dependence of the Raman modes of all phases, except the Raman-inactive disordered rocksalt phase, have been measured and discussed. © 2013 American Institute of Physics. [<http://dx.doi.org/10.1063/1.4794096>]

I. INTRODUCTION

Many compounds of the type $A^{\text{II}}B_2^{\text{III}}X_4^{\text{VI}}$, with A^{II} and B^{III} being divalent and trivalent metals, respectively, crystallize at ambient conditions in tetragonal structures derived from the diamond or zincblende (space group (S.G.) F-43m, No. 216, $Z=2$) structure. These compounds contain both A and B cations in tetrahedral coordination so there is an unbalanced number of cations and anions in the structure which leads to the appearance of vacancies in these structures. In most cases, the vacancies are located in fixed Wyckoff positions of the unit cell and so these compounds are called adamantine ordered-vacancy compounds (OVCs).

Adamantine OVCs constitute a class of semiconductors that exhibit extraordinary and unusual properties. The different number of anions and cations, unlike in the zincblende structure, implies that A and B cations are usually inequivalent tetrahedrally coordinated cations located in different Wyckoff sites. Consequently, the doubling of the cubic zincblende unit cell along the c axis in OVCs results in a tetragonal symmetry which provides them with special properties not present in cubic zincblende-type compounds. In particular, adamantine OVCs have important applications in optoelectronics, solar cells, and non-linear optics that have attracted considerable attention in the last thirty years, as evidenced in several reviews.¹⁻⁴

Mercury digallium sulfide (HgGa_2S_4) crystallizes at ambient conditions in the tetragonal defect chalcopyrite (DC) structure (S.G. I-4, No. 82, $Z=2$) as shown in Fig. 1(a).^{5,6} This semiconductor is of considerable interest because of its nonlinear optical properties in the mid-infrared (IR) spectral range, high nonlinear susceptibility coefficients, fairly good birefringence, and a wide transparency range from 0.5 to 13 μm .⁵⁻⁸ High values of laser threshold and conversion efficiency allow using this compound as frequency doubling, optical parametric oscillator (OPO), and optical parametric amplifier (OPA) in the wavelength range from 1.0 to 10 μm .⁹ The development of the technique of growing mercury thio-gallate crystals helped synthesize high-quality optical crystals, which offer the possibility of using them in OPOs pumped by radiation of widespread Nd:YAG lasers. Owing to the combination of their properties, this compound can occupy a leading position among the most promising nonlinear materials. Therefore, the good nonlinear properties and the optical quality of HgGa_2S_4 crystal allow this material to compete with AgGaS_2 , AgGaSe_2 , ZnGeP_2 , and GaSe crystals.¹⁰

Despite the strong interest in the characterization of the properties of HgGa_2S_4 , there is no study, to our knowledge, of its properties at high pressures probably due to the difficulties found in growing these crystals.¹¹ On the contrary, there are several measurements of the physical properties of other sulfide-based OVCs (ZnGa_2S_4 , CdGa_2S_4 , CdAl_2S_4 , and HgAl_2S_4) under pressure.¹²⁻¹⁶ In some of these works it has been shown that sulfide-based adamantine OVCs undergo a pressure-induced phase transition from the DC structure toward the disordered rocksalt (DR) structure, where cations

^{a)}Author to whom correspondence should be addressed. Electronic mail: rovilap@fis.upv.es.

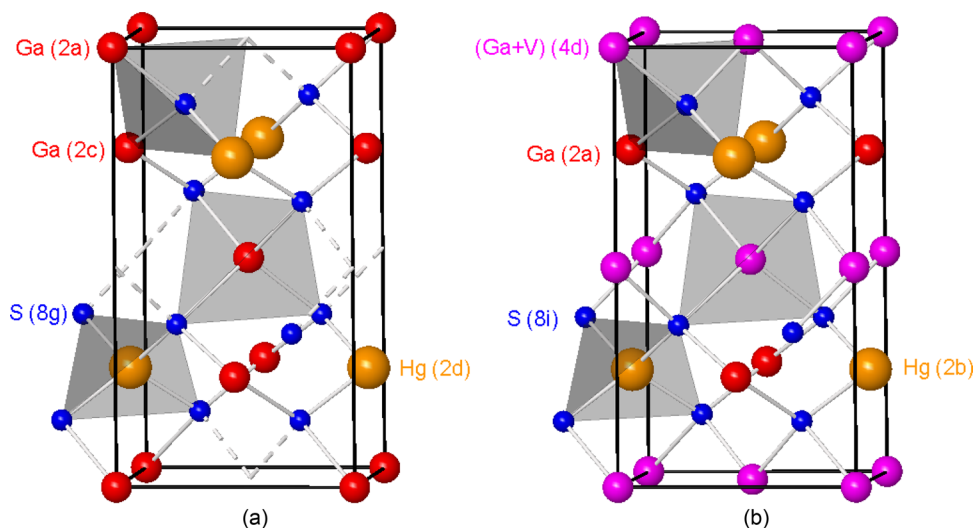


FIG. 1. Schematic view of the defect chalcopyrite structure (a) and defect stannite structure (b) of HgGa_2S_4 . Big (orange) atoms are Hg, medium (red) atoms are Ga, and small (blue) atoms are S. Medium (magenta) atoms represent the mixture of Ga and vacancy atoms.

and vacancies mix at the only available Wyckoff site for cations. This phase transition is related to the pressure-induced zincblende-to-rocksalt phase transition in many binary compounds and the pressure-induced phase transition from the chalcopyrite phase toward the DR phase in ternary chalcopyrites. In OVCs, like in chalcopyrites, this pressure-induced phase transition is an order-disorder transition since the DC structure is fully ordered and the DR structure is fully disordered. In this context, it was suggested that the adamantite OVCs should undergo a sequence of pressure-induced order-disorder transitions from a fully ordered structure towards a fully disordered structure through intermediate phases with partial disorder.^{13–15} Intermediate phases of disorder in pressure-induced order-disorder transitions were suggested on the basis of its observation in previous temperature-induced order-disorder phase transitions in OVCs. Typically, a defect stannite (DS) structure (S.G. I-42m, No. 121, $Z = 2$) was found between the fully ordered DC structure and the fully disordered zincblende (DZ) structure.^{3,17} However, till now there is no absolutely convincing report showing evidences of the intermediate phases with partial cation-vacancy disorder in OVCs under high pressure.

In order to improve the knowledge of the high-pressure behaviour of HgGa_2S_4 and the pressure-induced order-disorder processes involved in this compound at room temperature (RT), we have performed RT high-pressure Raman scattering measurements of DC- HgGa_2S_4 during three pressure cycles that have been complemented with lattice dynamics *ab initio* calculations. A DC-to-DS phase transition above 18 GPa was observed that evidences the presence of an intermediate phase with partial disorder between the DC and DR phases. The DS phase was quenched in a metastable way at low pressures on downstroke from 22 GPa and it was found to undergo a transition to the DR phase above 23 GPa. On decreasing pressure from 25 GPa, a metastable DZ phase was observed at low pressures. Therefore, our measurements show a compelling evidence of an intermediate phase between DC and DR phases and also the irreversibility of the order-disorder phase transitions in HgGa_2S_4 . Furthermore, the pressure dependence of

the Raman modes of the three Raman-active phases (DC, DS, and DZ) are reported and discussed.

II. EXPERIMENTAL SECTION

Samples used in the present study, were single crystals of DC- HgGa_2S_4 grown from its constituents HgS and Ga_2S_3 by chemical vapor transport method using iodine as a transport agent.¹⁸ Samples were loaded with a 16:3:1 methanol-ethanol-water mixture as a pressure-transmitting medium, which behaves quasihydrostatically till 25 GPa, in the 150 μm diameter hole of an Inconel gasket inside a membrane-type diamond anvil cell. Pressure was determined by the ruby luminescence method.¹⁹ The shape and separation of the R_1 and R_2 ruby lines were checked at each pressure and neither a significant increase in width nor an overlapping of both peaks were detected; thus suggesting that quasihydrostatic conditions are fulfilled up to the highest measured pressure. In any case, we can estimate the error in the pressure determination of about 0.1 GPa below 10 GPa, 0.2 GPa between 10 and 20 GPa, and 0.3 GPa above 20 GPa. These values are smaller than the sizes of symbols plotted in the figures representing the pressure dependence of the Raman mode frequencies.

High-pressure unpolarized Raman scattering measurements at RT were performed with a HORIBA-Jobin Yvon LabRAM HR UV microspectrometer coupled to a Peltier-cooled CCD camera and using a 632.81 nm (1.96 eV) HeNe laser excitation line with a power smaller than 10 mW and a spectral resolution better than 2 cm^{-1} . During Raman experiments samples were checked before and after each measurement in order to be sure that no radiation damage occurs during the measurements by the incoming laser excitation. In order to analyze the Raman spectra under pressure, Raman peaks have been fitted to a Voigt profile (Lorentzian profile convoluted by a Gaussian profile) where the spectrometer resolution is taken as a fixed Gaussian width.

As commented previously, we have pressurized the sample during three pressure cycles carrying out Raman

measurements both during upstroke and downstroke. The pressure values reached during the three pressure cycles were 22, 25, and 18 GPa, respectively. The reasons to choose these maximum pressures will be clarified in Sec. IV.

III. THEORETICAL CALCULATION DETAILS

Total energy and lattice dynamics calculations were performed within the framework of the density functional theory (DFT) and the pseudopotential method using the Vienna *ab initio* simulation package (VASP) of which a detailed account can be found in Ref. 20 and references therein. The exchange and correlation energy has been taken in the generalized gradient approximation (GGA), according to Perdew-Burke-Ernzerhof (PBE) prescription.²¹ Details of total energy calculations in the DC structure can be consulted in Refs. 22 and 23.

Total energy calculations were only performed for the DC structure. We have not calculated the DS and DZ phases of HgGa₂S₄ despite five possible DS phases for OVCs have been discussed by Eifler *et al.* and Gomis *et al.*^{23–25} The reason is that calculations with structures with fractional atomic occupations, like most DS and DZ phases with *ab initio* codes are of great difficulty (e.g., one can use a supercell to simulate disorder but calculations become very time consuming).

Lattice dynamics calculations of phonon modes were performed in the DC phase at the zone centre (Γ point) of the Brillouin zone (BZ). For the calculation of the dynamical matrix at the Γ point we used the direct method²⁶ which involves a separate calculation of the forces in which a fixed displacement from the equilibrium configuration of the atoms within the primitive unit cell is considered. Details of the lattice dynamics calculations can be consulted in Ref. 23. In order to include the transversal-longitudinal optic (TO-LO) splitting in our study, we need to add the effect of the electric field that it is not included in the previous direct force method. To evaluate the phonons at the Γ point the calculations were carried out in the framework of density functional perturbation theory (DFPT)²⁷ with the Quantum Espresso package.²⁸ We add the non-analytic term due to the long-range interaction using the response of the system to the electric field; it allows us to obtain the TO-LO splitting near the Γ point along the directions (100) or (010) and (001). Therefore, we can calculate the pure B and E modes with TO and LO splitting. For these calculations, we used ultrasoft pseudopotentials with a cutoff of 60 Ry, a big sampling of k-special points to obtain well converged results, and the same exchange correlation prescription used in the total energy and lattice dynamics calculations.

IV. RESULTS AND DISCUSSION

A. First upstroke

According to group theory,²⁹ the DC structure of HgGa₂S₄ should have twenty-one optical vibrational modes at Γ with the mechanical representation

$$\Gamma = 3A \oplus 5B(\text{R, IR}) \oplus 5E(\text{R, IR}) \oplus B \oplus E, \quad (1)$$

where *A* modes are non-polar modes, and *B* and *E* modes are polar modes, being *E* modes doubly degenerated. This results in a total of thirteen Raman-active (R) modes ($3A \oplus 5B \oplus 5E$) and ten IR modes ($5B \oplus 5E$) since one *B* and one *E* are acoustic modes. It is interesting to note that doubly degenerate *E* modes correspond to vibrations of atoms along the *a* and *b* axis; i.e., in the directions perpendicular to the *c* axis, while *B* modes correspond to vibrations of atoms along the *c* axis. In addition, two wavenumbers (either R or IR) should be observed for each *B* and *E* modes in the DC structure due to the TO-LO splitting of the polar modes. Consequently, taking into account the TO-LO splitting, up to twenty-three Raman-active modes and twenty IR-active modes could be observed in DC-HgGa₂S₄.

Figure 2(a) shows the RT Raman spectra of DC-HgGa₂S₄ up to 20.2 GPa. The Raman spectrum can be divided into three regions: (i) the low-frequency region below 200 cm⁻¹, (ii) the medium-frequency region between 200 and 300 cm⁻¹, and (iii) the high-frequency region above 300 cm⁻¹. The modes in the low- and medium-frequency region are in general more intense than those in the high-frequency region. The most intense peak of the Raman spectrum of DC-HgGa₂S₄, as in other DC compounds, is the *A*¹ mode; i.e., the “breathing” mode associated to the symmetric oscillation of the anions against the stoichiometric vacancy. Raman mode symmetries were assigned with the help of our *ab initio* calculations. It can be observed that *A* modes are in the medium- and high-frequency region, whereas the *B* and *E* modes mainly spread along the low- and high-frequency regions, with the exception of the *E*³ mode which is in the medium-frequency region very close to the *A*¹ mode.

We have followed the pressure dependence of 15 Raman-active modes and we have measured the TO-LO splittings in DC-HgGa₂S₄ that correspond to *E*¹, *E*⁴, and *E*⁵ modes. The only first-order Raman-active mode not followed is the weak *B*³ mode.^{30–32} It can be observed that above 18 GPa there are three extra Raman peaks marked with asterisks in Fig. 2(a) that suggest the occurrence of a phase transition to the DS structure which will be commented later. Figure 2(b) shows the pressure dependence of the experimental (symbols) and theoretical (lines) Raman mode frequencies of DC-HgGa₂S₄ up to 20 GPa. It can be observed that the peaks in the medium- and high-frequency regions shift to higher frequencies as pressure increases while most of the peaks of the low-frequency region show a negligible, very small, or even negative pressure coefficient.

The experimental and theoretical Raman mode symmetries, frequencies at zero pressure, and pressure coefficients at zero pressure, as obtained from fits to the data using $\omega = \omega_0 + aP$ or $\omega = \omega_0 + aP + bP^2$ equations, are summarized in Table I. Our experimental Raman mode frequencies at zero pressure are compared to those reported in previous works.^{30–32} In general, a good agreement between the different experimental values at zero pressure is observed as well as the theoretical and experimental frequencies and pressure coefficients. This agreement supports the symmetry assignment of the experimental modes on the basis of our theoretical calculations. In this context, we have assigned the low-frequency modes below 220 cm⁻¹ in the same way as

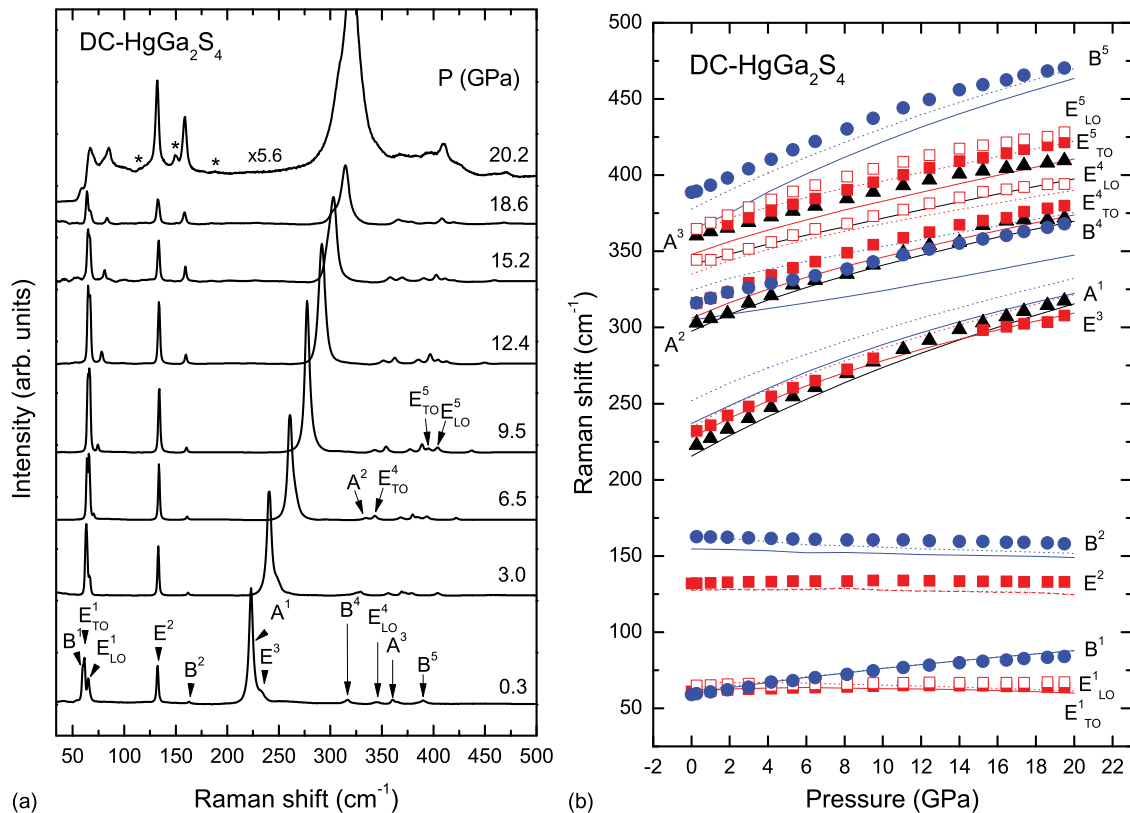


FIG. 2. (a) RT Raman spectra of DC-HgGa₂S₄ up to 20.2 GPa during the 1st upstroke. (b) Pressure dependence of the experimental (symbols) and calculated (lines) vibrational modes in DC-HgGa₂S₄ during the 1st upstroke. Experimental values of A, B_{TO}/B_{LO} and E_{TO}/E_{LO} Raman modes are represented by solid triangles (black), solid/open circles (blue), and solid/open squares (red), respectively. Theoretical calculations for the TO (LO) phonons of pure B and E symmetry are represented by solid (dotted) lines with blue and red colors, respectively, while modes of A symmetry are represented by solid black lines. Pressure uncertainty is smaller than the symbols' size.

previous works.^{30–32} However, there are different assignments of symmetry in the Raman modes above this frequency. These discrepancies are common in the literature of AB_2X_4 compounds in the high-frequency region because of the overlapping of relatively broad and weak modes. However, the strongest discrepancies that we have found between the experimental Raman works of HgGa₂S₄ are related to the A² and A³ modes, which are characteristic modes of the DC structure and are usually well established in the literature of AB_2X_4 compounds. We have assigned these two A modes to Raman features at 300 and 358 cm⁻¹, respectively, on the basis of the comparison of the experimental and theoretical frequencies and pressure coefficients. Curiously, these two Raman-active modes were not reported by Haeuseler³⁰ and were reported by Razzetti and Lottici at 318 and 365 cm⁻¹, respectively.³² The mode at 318 cm⁻¹ is close to the modes, we have measured at 315 and 316 cm⁻¹ (that Haeuseler *et al.* report at 323 and 324 cm⁻¹) and that can be attributed to E⁴ and B⁴ modes on the basis of their frequencies and pressure coefficients that agree with polarization measurements of Haeuseler *et al.*^{30,31} On the other hand, the mode at 365 cm⁻¹ is close to our modes of 360 and 364 cm⁻¹ (that Haeuseler *et al.* report at 363 cm⁻¹) and that can be attributed to the E⁵ mode.

Finally, another discrepancy between the experimental works is the symmetry assignment of the high-frequency modes. Razzetti and Lottici attributed the two Raman modes

of highest frequency to mixed Raman modes of B and E symmetry of TO and LO character, respectively. Instead, we have attributed the Raman mode of highest frequency only to the B⁵ mode on the basis of its frequency and pressure coefficient. In this respect, we have to note that for the assignment of the symmetries of the Raman-active modes it must be taken into account that DC and DS compounds are optically uniaxial crystals. This means that, except for incidence along the optical axis or at 90° from it, symmetry or character coupling is to be expected for Raman modes.^{33,34} Thus, one may observe E, B, LO, and TO quasimodes, resulting from the coupling of E_{TO} + E_{LO}, B_{TO} + B_{LO}, E_{TO} + B_{TO}, or E_{LO} + B_{LO} modes. These couplings depend on the relative magnitude of polar (LO-TO) versus anisotropy (B-E) splitting for each B-E pair of modes. In particular, when Raman scattering is measured with laser incidence along the (111) plane, which is the direction perpendicular to the typical cleavage plane of OVCs one does not expect to observe pure E or B modes but quasimodes. Therefore, the comparison of experimental and theoretical data, which provide pure E and B modes and pure TO and LO modes, must be done with caution. In our particular case for DC-HgGa₂S₄, it seems that the highest-frequency mode shows a frequency and pressure coefficient very close to that of the theoretical B⁵_{LO} mode; thus, we have attributed this mode only to B⁵_{TO + LO} symmetry. Furthermore, the observation of three modes above 358 cm⁻¹ seems to exclude E_{TO} + B_{TO} or E_{LO} + B_{LO} modes;

TABLE I. Experimental (exp.) and calculated (th.) Raman-mode frequencies at room pressure and their pressure coefficients in DC-HgGa₂S₄ as obtained from fits to the data using ($\omega = \omega_0 + aP$) or ($\omega = \omega_0 + aP + bP^2$) equations during the 1st pressure cycle where b was multiplied by a factor 100.

Mode symmetry (th.)	ω_0 (th.) (cm ⁻¹)	a (th.) (cm ⁻¹ GPa ⁻¹)	b (th.) $\times 100$ (cm ⁻¹ GPa ⁻²)	Mode symmetry (exp.)	ω_0 (exp.) (cm ⁻¹)	a (exp.) (cm ⁻¹ GPa ⁻¹)	b (exp.) $\times 100$ (cm ⁻¹ GPa ⁻²)	ω_0 (exp.) (cm ⁻¹)
E^1 (TO)	64(1)	-0.14(3)		E^1 (TO)	62(1)	0.16(3)		61 ^c ,63 ^{a,b}
E^1 (LO)	68(1)	-0.3(1)		E^1 (LO)	65(1)	0.10(1)		68 ^{b,c}
B^1 (TO)	61(1)	1.4(1)		B^1 (TO)	61(1)	1.3(5)		59 ^b
B^1 (LO)	62(1)	1.3(1)		B^1 (LO)				63 ^b
E^2 (TO)	128(1)	-0.14(4)		E^2 (TO)	133(1)	0.04(2)		132 ^b ,134 ^{a,c}
E^2 (LO)	129(1)	-0.16(3)		E^2 (LO)				133 ^b
B^2 (TO)	155(1)	-0.3(1)		B^2 (TO)	163(1)	-0.2(1)		160 ^c ,166 ^b
B^2 (LO)	162(1)	-0.5(1)		B^2 (LO)				167 ^c ,170 ^b
A^1	216(2)	6.6(3)	-8(2)	A^1	220(1)	7.0(1)	-10(2)	223 ^c ,224 ^a
E^3 (TO)	229(2)	6.0(3)	-10(3)	E^3 (TO)	230(2)	6.3(1)	-12(2)	234 ^b ,235 ^c
E^3 (LO)	236(2)	5.9(3)	-8(2)	E^3 (LO)				237 ^b
B^3 (TO)	237(2)	6.1(3)	-9(2)	B^3 (TO)				252 ^b ,254 ^a
B^3 (LO)	253(2)	5.2(3)	-7(2)	B^3 (LO)				257 ^b
A^2	299(2)	5.0(3)	-7(2)	A^2	300(2)	5.1(1)	-7(1)	318 ^c
B^4 (TO)	305(2)	1.8(1)	1.9(1)	B^4 (TO)	316(3)	3.0(1)	-2(1)	323 ^b
B^4 (LO)	326(2)	3.1(2)	-3(1)	B^4 (LO)				342 ^b
E^4 (TO)	307(2)	4.6(2)	-6(2)	E^4 (TO)	315(4)	4.9(3)	-7(1)	324 ^b
E^4 (LO)	336(2)	3.8(2)	-6(2)	E^4 (LO)	341(3)	3.9(2)	-6(1)	345 ^b , 349 ^c
A^3	342(2)	3.3(2)	-3(1)	A^3	358(2)	3.7(1)	-6(1)	365 ^c
E^5 (TO)	349(2)	3.8(2)	-4(1)	E^5 (TO)	360(3)	4.3(2)	-6(1)	363 ^a ,372 ^c
E^5 (LO)	362(2)	4.0(2)	-5(1)	E^5 (LO)	364(3)	3.2(2)	-10(2)	383 ^b ,386 ^c
B^5 (TO)	364(2)	6.7(3)	-8(2)	B^5 (TO)	387(4)	6.1(3)	-9(2)	369 ^b ,372 ^c
B^5 (LO)	378(2)	6.0(3)	-7(2)	B^5 (LO)				385 ^b ,388 ^a

^aReference 29.^bReference 30.^cReference 31.

otherwise, only two modes should have been observed in this frequency region.

In order to obtain more information on the pressure-induced order-disorder processes, we have analyzed (not shown) the pressure dependences of the Raman mode intensities and linewidths as previously done in other high-pressure studies of OVCs.^{13,14,23} No clear information on the order-disorder processes can be obtained from the pressure dependence of these data; however, it is interesting to note that there is a small increase of the intensity of the A^3 mode normalized to that of the A^1 mode with pressure. This fact is similar to that previously observed in CdAl₂S₄¹³ and in CdGa₂Se₄,²³ where this behaviour related to the transformation from the DC to the DS phase since it is coincident with the simultaneous decrease of the intensity of the A^2 mode (the mode that disappears at the DC-to-DS transition). Unfortunately, the pressure-dependence of the intensity of the A^2 mode is difficult to follow in the Raman spectrum of DC-HgGa₂S₄ since this mode has a decreasing intensity along the series ZnGa₂S₄, CdGa₂S₄, HgGa₂S₄ (Ref. 14) and overlaps with the B^4 and E^4 modes above 10 GPa.

As already mentioned, three new modes appear in the Raman spectrum above 18 GPa [see asterisks in Fig. 2(a)]. These new peaks can correspond either to a new phase coexisting with the original DC phase or to a new phase showing similar but more Raman peaks than the original DC phase. In order to resolve whether there is only one or two phases

above 18 GPa, we followed the evolution of the spectrum up to 22 GPa. Along this pressure range we observed no further changes occurred in the spectrum which indicated the disappearance of the Raman modes of the original DC phase nor the appearance of new modes of the high-pressure phase, and we decreased pressure to almost ambient pressure to check the reversibility of the changes observed in the Raman spectrum. Figure 3 shows the comparison of the Raman spectra around 3 GPa during the first upstroke and second upstrokes. It can be observed that the new peaks appearing during the first upstroke above 18 GPa are still observed after decreasing pressure to almost ambient pressure. Furthermore, a close comparison of the linewidth of the Raman peaks during the first and second upstroke reveal that some peaks get broadened while others do not. In particular, the broadening of the most intense A mode and of the high-frequency modes suggests that the recovered sample corresponds to the DS phase rather than to the original DC phase.³⁵ Note that the broadening of many Raman modes in the spectrum of the DS phase with respect to the spectrum of the DC phase was also evidenced in CdGa₂Se₄,²³ and in ZnGa₂Se₄.²⁵ In summary, all these results indicate that above 18 GPa the original DC sample undergoes an irreversible phase transition toward a DS phase showing more Raman modes.

A recent paper reporting Raman measurements on CdGa₂Se₄ under pressure has suggested that CdGa₂Se₄

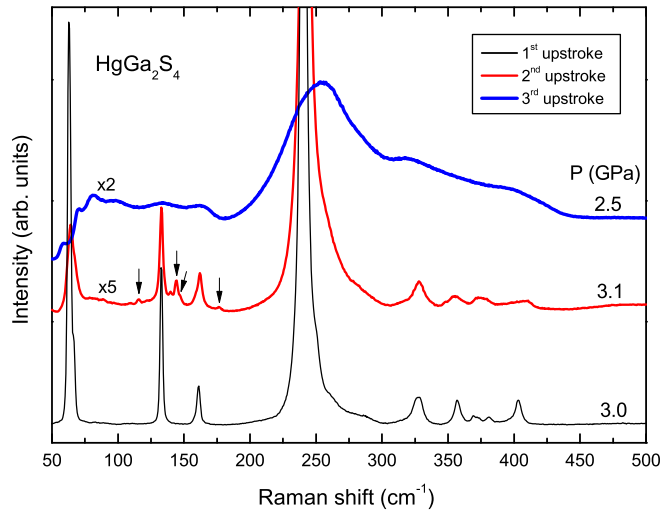


FIG. 3. Comparison of the Raman spectra of the DC-, DS- and DZ-HgGa₂S₄ crystals at different pressures during the 1st, 2nd, and 3rd upstrokes at pressures of 3.0, 3.1, and 2.5 GPa, respectively. Arrows indicate the new Raman modes observed in the DS phase.

undergoes a DC-to-DS pressure-induced phase transition prior to the transition toward the DR phase.²³ In that paper it was claimed that there are several possible phases, DS phases and disordered CuAu-like (DCA) layered phases, with an intermediate degree of cation or cation-vacancy disorder between that of the completely ordered DC phase and that of the completely disordered DZ and DR phases. In that work, it was suggested that there are two possible DS polytypes (models 4 and 5) with more Raman peaks than the DC phase because of the atomic occupation of the $2b$ Wyckoff site [occupied by the vacancy in the DC structure, see Fig. 1(a)]. In particular, these two DS phases should exhibit one B mode and one E mode more than the DC phase, but one A mode less than the DC phase; i.e., up to three extra Raman modes could be observed in the DS phase compared to the DC phase if we take into account the TO-LO splitting. This fact could be consistent with the observation of some new Raman modes above 18 GPa in HgGa₂S₄.

In order to find out which one of the two possible DS phases (models 4 and 5) could correspond to the high-pressure phase of HgGa₂S₄, we have analyzed the different probabilities of the two models. It is easy to understand that model 4 has a higher probability to occur than model 5 (Ref. 23). In model 4, Ga cations and vacancies initially at $2a$ and $2b$ sites of the DC structure [Fig. 1(a)], respectively, get mixed in the same cation plane perpendicular to the c axis leading to a $4d$ site in the DS structure [Fig. 1(b)]. On the contrary, in model 5, vacancies at $2b$ sites and Ga cations at $2a$ and $2c$ sites of the DC structure get mixed. Since Ga cations at $2c$ sites are in a different cation plane perpendicular to the c axis than vacancies, the probability of occurrence of model 5 of the DS phase upon disorder of the DC phase is a little bit smaller than that of model 4 because in model 5 vacancies must mix with cations in the two different cation planes, while in model 4 vacancies mix only with cations corresponding to the same cation plane. Therefore, on the view of the different probabilities of the two models, we

tentatively propose that the DS phase observed in HgGa₂S₄ above 18 GPa could correspond to model 4 shown in Fig. 1(b).

A possible justification for the observation of polytype 4 of the DS phase instead of model 2, more common in Zn-based compounds,^{25,35–37} is that Hg (A cation) is rather larger compared to Ga (B cation); therefore, the mix of Hg and Ga cations at the same cation plane can be difficult. This would avoid the formation of model 2 of the DS phase²³ and would lead to the more favorable mixing of Ga cations and vacancies at the same cation plane resulting in model 4 of the DS phase.²³ The case of HgGa₂S₄ is the opposite to the case of ZnGa₂S₄ and ZnGa₂Se₄, where model 2 is the assumed DS phase occurring at ambient conditions because it is easy for Zn and Ga atoms with similar sizes to get mixed.^{25,35–37}

B. Second upstroke

As already commented, the first thing we noted on decreasing pressure from 22 GPa was the non-reversibility of the phase transition occurring above 18 GPa (see Fig. 3). This result allowed us to characterize the Raman spectrum of the new phase till 23 GPa during a second upstroke.

According to group theory, if we assume model 4 for the new DS phase, the DS structure of HgGa₂S₄ should have twenty-four optical vibrational modes at Γ with the mechanical representation²⁹

$$\Gamma = 2A_1(\text{R}) \oplus A_2 \oplus 2B_1(\text{R}) \oplus 4B_2(\text{R, IR}) \oplus 6E(\text{R, IR}) \oplus B_2 \oplus E, \quad (2)$$

where B_2 and E are polar modes, being E modes doubly degenerated. This results in a total of fourteen Raman-active modes ($2A_1 \oplus 2B_1 \oplus 4B_2 \oplus 6E$) because the A_2 mode is silent, and ten IR-active modes ($4B_2 \oplus 6E$), since one B_2 and one E are acoustic modes. In addition, two modes (either in R or IR) should be observed for each B_2 and E modes in the DS structure, due to the transversal-longitudinal optic (TO-LO) splitting of the polar modes. Consequently, taking into account the TO-LO splitting, up to twenty-four Raman-active modes could be observed in the DS phase. Note that the same number of Raman-active modes is expected for model 5 of the DS phase so no discrimination between models 4 and 5 of the DS phase can be done *a priori* on the basis of Raman scattering arguments.²³

Figure 4(a) shows the Raman spectra of DS-HgGa₂S₄ from 1 to 25 GPa. Up to seventeen Raman-active modes of the DS phase were observed till 23 GPa. Above this pressure, a transition to a Raman-inactive phase occurs, which we have attributed to the DR phase already observed in high-pressure studies of other OVCs.^{15,16,23,36,38} Some of the Raman-active modes of the DS phase are very similar to those of the parent DC phase (see Fig. 3). Figure 4(b) shows the pressure dependence of the Raman-active mode frequencies of DS-HgGa₂S₄ from 1 to 23 GPa. The frequencies at zero pressure and the pressure coefficients of the experimental modes in DS-HgGa₂S₄ are reported in Table II. It can be observed that the pressure coefficients of the Raman-active

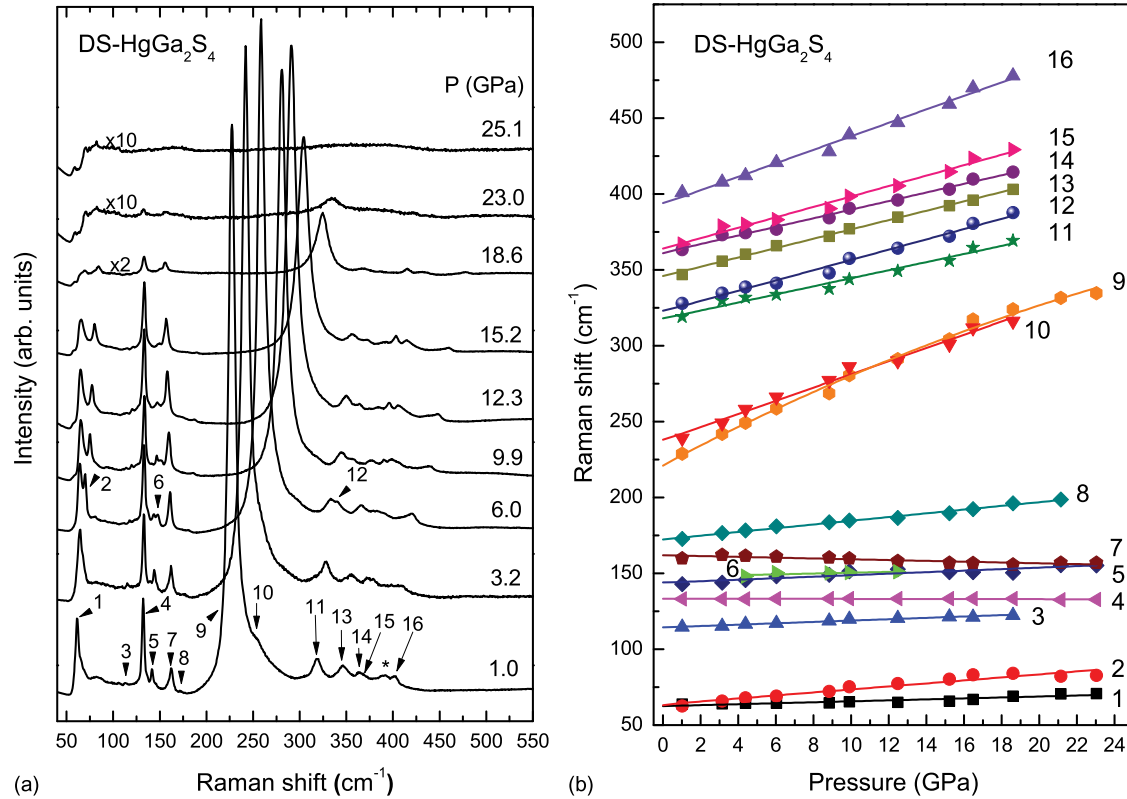


FIG. 4. (a) RT Raman spectra of DS-HgGa₂S₄ up to 25.1 GPa during the 2nd upstroke. (b) Pressure dependence of the experimental (symbols) vibrational modes in DS-HgGa₂S₄ during the 2nd upstroke. Pressure uncertainty is smaller than the symbols' size.

modes of the DS phase are also similar to those of the DC phase. Unfortunately, we have not been able to perform calculations with model 4 of the DS phase to help us in the symmetry assignment of the Raman-active modes of the DS phase, as already commented. Therefore, we provide in Table II a tentative assignment of the Raman mode symmetries which is made on the basis of the frequencies and

TABLE II. Experimental (exp.) Raman-mode frequencies and pressure coefficients observed in DS-HgGa₂S₄ at RT as obtained from fits to the data using $(\omega = \omega_0 + aP)$ or $(\omega = \omega_0 + aP + bP^2)$ equations during the 2nd pressure cycle where b was multiplied by a factor 100.

Modes	Mode symmetry	ω_0 (exp.) (cm ⁻¹)	a (exp.) (cm ⁻¹ GPa ⁻¹)	b (exp.) ($\times 100$) (cm ⁻¹ GPa ⁻²)
1	E ¹	62(1)	0.3(1)	
2	B ₁ ¹	63(1)	1.0(1)	
3		114(3)	0.5(2)	
4	E ²	133(1)	-0.02(1)	
5	E ³ (TO)	144(1)	0.5(2)	
6	E ³ (LO)	148(1)	0.3(2)	
7	B ₂ ¹	162(1)	-0.3(1)	
8	B ₂ ²	172(1)	1.2(4)	
9	A ₁ ¹	221(3)	6.5(1)	-6(2)
10	E ⁴	238(2)	4.4(3)	
11	B ₁ ²	318(2)	2.6(1)	
12	E ⁵ (TO)	323(2)	3.4(2)	
13	E ⁵ (LO)	347(2)	3.1(3)	
14	A ₁ ²	361(2)	3.8(2)	
15	E ⁶	364(3)	3.4(3)	
16	B ₂ ⁴	394(2)	4.4(2)	

pressure coefficients of the different Raman modes and its comparison with the Raman-active modes observed in the DC phase (see Sec. IV A) and with the assignment of Raman-active modes already performed in DS-ZnGa₂Se₄.³⁵

In this respect, the low-frequency modes 1 and 2 of the DS phase are similar to those of the DC phase and are assigned to the E¹ and B₁¹ modes. Similarly, modes 4 and 7 correlate with those of the DC phase and can be attributed to the E² and B₂¹ modes, respectively. The weak mode 3, whose pressure coefficient is very small, is the only mode we have not been able to assign. On the other hand, the modes 5 and 6 are likely to be the TO and LO components of the new E mode of the DS phase not present in the DC phase; i.e., the E³ mode. Finally, mode 8 can be attributed to the new B₂ mode of the DS phase with respect to the DC phase; i.e., the B₂² mode.

In the medium-frequency region, modes 9 and 10 can be safely attributed to modes A₁¹ and E⁴ of the DS phase because they show similar pressure dependence that those of the DC phase in the medium-frequency region. The B₂³ mode is not observed in this region in the same way that the B³ mode of the DC phase is not observed in this region. As regards the high-frequency region, mode 11 is likely to be the B₁² mode which shows a similar pressure dependence than that of the B⁴ mode in the DC phase. Modes 12 and 13 of the DS phase are likely to be the TO and LO components of the E⁵ mode since both components have been observed in the E⁴ mode of the DC phase. Mode 14 can be attributed to the A₁² mode because it is similar to the A³ mode in the DC phase; i.e., it has a similar frequency and the smallest

pressure coefficient in this frequency region. Mode 15 is attributed to the E^6 mode since it shows a similar behavior than the E^5 mode of the DC phase. Finally, mode 16 can be safely attributed to the B_2^4 mode because they behave in a similar way than the B^5 mode in the DC phase. The asterisk before the mode 16 represents a mode that it was not possible to follow under pressure so we have not been able to venture its nature.

C. Third upstroke

After undergoing the DS-to-DR phase transition above 23 GPa during the second upstroke we arrived till 25 GPa. At this pressure, we checked that the transition to DR phase was completed everywhere in the sample by measuring in different sample zones. On decreasing the pressure from 25 GPa till almost ambient pressure the Raman spectrum of the DS phase was not recovered, thus indicating that the DS-to-DR phase transition is not reversible in HgGa_2S_4 . Instead, we observed a Raman spectrum with broad bands (see top spectrum of Fig. 3) which compares with the relatively narrow Raman modes of the DC and DS phases. Raman spectrum on downstroke cannot be attributed to the DR phase, which is Raman inactive, but also it cannot correspond neither to the DC phase nor to the DS phase. Since the DR phase is a totally disordered phase, we have tentatively attributed the Raman spectrum on downstroke to the totally DZ phase, as we did for CdGa_2Se_4 .²³ This result is also in agreement with results of many authors that have observed the DZ phase on decreasing pressure in several defect chalcopyrites.^{15,16,38}

Figure 3 shows that the Raman spectrum of the recovered sample is rather continuous and looks like a one-phonon density of states (1PDOS). The Raman spectrum of DZ- HgGa_2S_4 cannot be compared with the experimental 1PDOS of zincblende-type β - HgS but it can be compared to recent theoretical calculations of its 1PDOS.³⁹ It can be noted that the lowest-frequency edge of the TO branch at the 1PDOS of β - HgS (220 cm^{-1}) agrees well with the edge of the TO region for DZ- HgGa_2S_4 ; however, while in β - HgS the highest-frequency edge of the LO branch is near 300 cm^{-1} , the maximum value of phonons is around 415 cm^{-1} in DZ- HgGa_2S_4 near room pressure. In this respect, we have to note that the LO modes associated to Ga-S vibrations in Ga_2S_3 are above 430 cm^{-1} (Ref. 40). Therefore, the observation of the Raman edge of the LO branch of DZ- HgGa_2S_4 above 400 cm^{-1} is indicative that the LO modes are dominated by Ga-S bonds rather than by Hg-S bonds what is consistent with the double number of Ga-S than Hg-S bonds in this OVC.

Figure 5(a) shows the Raman spectra of DZ- HgGa_2S_4 on increasing pressure till 18.4 GPa during the third upstroke since the sample transitioned again to the DR phase above this pressure. We have marked up to ten features in the Raman spectra that can be followed under pressure and whose pressure dependences are plotted in Fig. 5(b). The frequencies at zero pressure and the pressure coefficients of the experimental modes in DZ- HgGa_2S_4 are reported in Table III. High-frequency modes in DZ- HgGa_2S_4 present higher linear pressure coefficients than the low-frequency modes. This

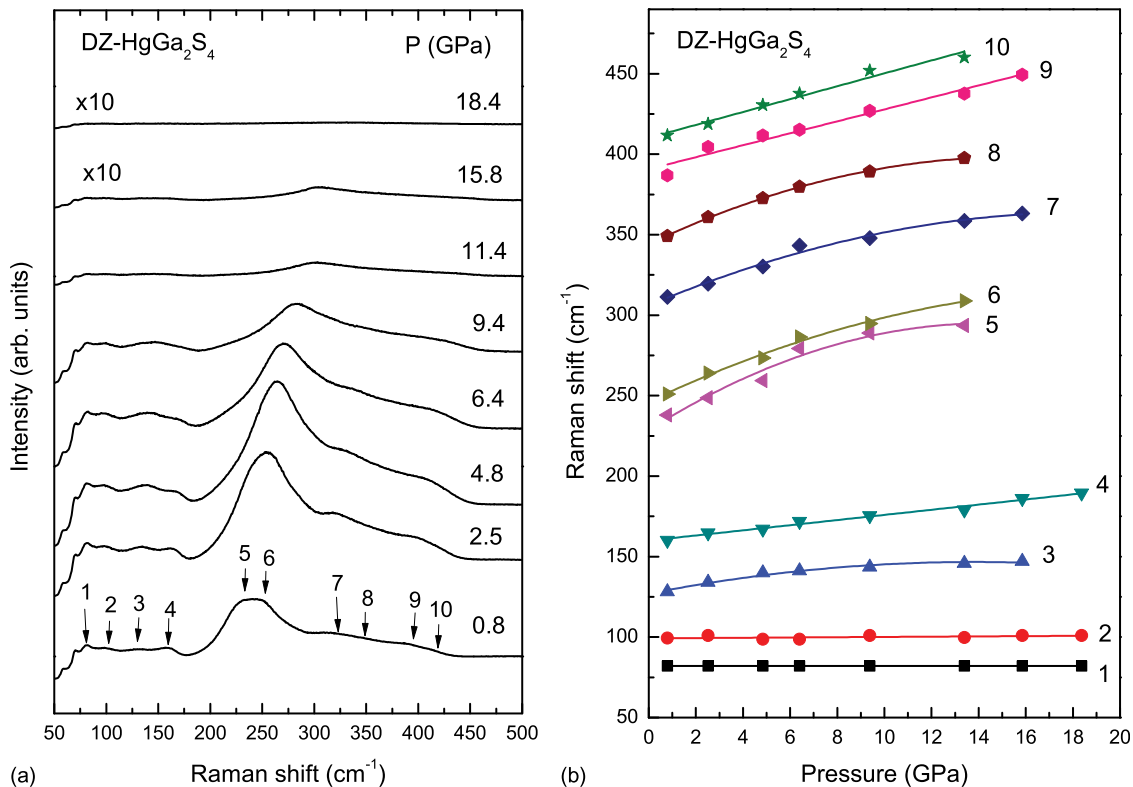
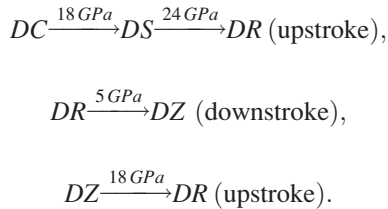


FIG. 5. (a) RT Raman spectra of DZ- HgGa_2S_4 up to 18.4 GPa during the 3rd upstroke. (b) Pressure dependence of the experimental (symbols) vibrational modes in DZ- HgGa_2S_4 during the 3rd upstroke. Pressure uncertainty is smaller than the symbols' size.

behavior is similar to that of Raman modes in both DC and DS phases previously described. In general, we have found that the maximum values of the pressure coefficients are smaller in the DZ phase than in the DC and DS phases, so it can be concluded that pressure coefficients have decreased as disorder has increased in HgGa₂S₄. A similar conclusion was already provided in a recent high-pressure study in CdGa₂Se₄.²³

As regards the assignment of the different features observed in Fig. 5(a), features 1 and 2 are close in energy to the E^1 and B^1 modes of the DC phase and have almost a negligible pressure coefficient; therefore, they should correspond to TA modes of the DZ phase. Features 3 and 4 correlate in energy with E^2 and B^2 modes of the DC phase and have a slightly positive pressure coefficient that should correspond to LA modes of the DZ phase. Features 5 and 6 are in the energy range of A^1 and E^3 modes of the DC phase and should correspond to the low-frequency edge of the TO branch of the DZ phase. Features 7–10 correlate in energy with the high-frequency modes of the DC phase and correspond to the optical branch of the DZ phase. In particular, feature 10 defines the high-frequency edge of the LO branch of the DZ phase already commented.

To finish we would like to summarize the sequences of pressure-induced phase transitions observed in DC-HgGa₂S₄.



The sequence of phase transitions in DC-HgGa₂S₄ is similar to that proposed earlier for DC-CdGa₂Se₄ but for both OVCs the intermediate DS phase observed on upstroke does not correspond to the same polytype on the basis of the different number of Raman modes measured for this intermediate phase. Also in analogy to what was found in DC-CdGa₂Se₄,²³ we would like to mention that the changes

TABLE III. Experimental (exp.) Raman-mode frequencies and pressure coefficients observed in DZ-HgGa₂S₄ at RT as obtained from fits to the data using ($\omega = \omega_0 + aP$) or ($\omega = \omega_0 + aP + bP^2$) equations during the 3rd pressure cycle where b was multiplied by a factor 100.

Mode symmetry	ω_0 (exp.) (cm ⁻¹)	a (exp.) (cm ⁻¹ .GPa ⁻¹)	b (exp.) (×100) (cm ⁻¹ .GPa ⁻²)
1	82(2)	0	
2	99(3)	0.08(6)	
3	127(4)	2.8(4)	-10(2)
4	160(3)	1.6(1)	
5	229(5)	2.9(2)	-30(10)
6	246(3)	6.9(9)	-17(6)
7	306(4)	6.2(8)	-17(5)
8	344(6)	7.0(2)	-22(1)
9	391(4)	3.7(3)	
10	410(3)	4.0(3)	

induced by pressure in the structure of the DC-HgGa₂S₄ correlate qualitatively with changes induced by pressure in the color and hence the direct bandgap of the sample (to be published elsewhere). While original DC-HgGa₂S₄ sample presents a pale yellow color, the sample darkens considerably above 17.8 GPa. A complete darkening occurs upon transition to the opaque metallic DR phase. Finally, on decreasing pressure from the metallic DR phase the sample recovers its transparency below 5 GPa but the sample shows a reddish color, which can be attributed to the DZ phase evidenced by Raman scattering.

V. CONCLUSIONS

We have performed Raman scattering measurements in DC-HgGa₂S₄ under high pressure and have compared our experimental results with *ab initio* calculations. Our measurements present for the first time the pressure dependence of the Raman-active modes of DC-HgGa₂S₄. Above 18 GPa an increase of the cation-vacancy disorder in the defect chalcopyrite phase is observed that results in a phase transition to a structure prior to the phase transition to the disordered rocksalt phase; i.e., an intermediate phase between the DC and DR phases. We have tentatively attributed the intermediate high-pressure phase to the DS phase (model 4) on the basis of disorder probability and of its Raman spectrum which shows more Raman peaks than the DC phase. The observation of polytype 4 of the DS phase contrasts with the intermediate DS phase (model 2) suggested to occur (on the basis of the disappearance of the A^2 Raman mode of the DC phase) in ZnGa₂Se₄ and ZnGa₂S₄ at room conditions and in CdGa₂Se₄ and CdGa₂S₄ at high pressures. In summary, the presence of an intermediate phase between DC and DR is clearly evidenced for the first time thanks to Raman scattering measurements that have provided further arguments that support the DC to DS phase transition, so difficult to characterize by X-ray diffraction measurements in ternary OVCs.

The pressure dependence of the Raman-active modes of the intermediate DS phase was characterized during a second pressure cycle and it was evidenced that the DS phase is stable till 23 GPa where it undergoes an irreversible phase transition to the DR phase. On decreasing pressure from 25 GPa, a DZ phase is recovered below 5 GPa. The pressure dependence of the Raman mode frequencies of the DZ phase were measured during a third upstroke till 18 GPa, pressure at which a reversible phase transition to the DR phase takes place. Therefore, this work evidences the irreversibility of the pressure-induced order-disorder DC-to-DR and DS-to-DR phase transitions and the complete reversibility of the DZ-to-DR phase transition in which no reordering process is involved.

ACKNOWLEDGMENTS

This study was supported by the Spanish government MEC under Grant No: MAT2010-21270-C04-01/03/04, by MALTA Consolider Ingenio 2010 project (CSD2007-00045), and by the Vicerrectorado de Investigación y Desarrollo of the Universidad Politécnica de Valencia

(UPV2011-0914 PAID-05-11 and UPV2011-0966 PAID-06-11). E. P.-G., P.R.-H., and A.M. acknowledge computing time provided by Red Española de Supercomputación (RES) and MALTA-Cluster. J.A.S. acknowledges Juan de la Cierva fellowship program for his financial support.

- ¹A. MacKinnon, in *Tables of Numerical Data and Functional Relationships in Science and Technology*, edited by O. Madelung, M. Schulz, and H. Weiss (Springer-Verlag, Berlin, 1985), Vol. 17, p. 124.
- ²A. N. Georgobiani, S. I. Radautsan, and I. M. Tiginyanu, *Sov. Phys. Semicond.* **19**, 121 (1985).
- ³J. E. Bernard and A. Zunger, *Phys. Rev. B* **37**, 6835 (1988).
- ⁴X. Jiang and W. R. L. Lambrecht, *Phys. Rev. B* **69**, 035201 (2004).
- ⁵H. Hahn, G. Frank, W. Klinger, A. Störger, G. Störger, and Z. Anorg. Z. *Anorg. Allg. Chem.* **279**, 241 (1955).
- ⁶H. Schwer and V. Krämer, *Z. Kristallogr.* **190**, 103 (1990).
- ⁷B. F. Levine, C. G. Bethea, H. M. Kasper, and F. A. Thiel, *IEEE J. Quantum Electron.* **12**, 367 (1976).
- ⁸V. V. Ursaki, P. C. Ricci, I. Tiginyanu, A. Anedda, N. N. Syrbu, and V. E. Tezlevan, *J. Phys. Chem. Solids* **63**, 1823 (2002).
- ⁹F. Rotermond, V. Petrov, and F. Noack, *Opt. Commun.* **185**, 177 (2000).
- ¹⁰V. V. Badikov, N. V. Kuzmin, V. B. Laptev, A. L. Malinovsky, K. V. Mitin, G. S. Nazarov, E. A. Ryabov, A. M. Seryogin, and N. I. Shchebetova, *Quantum Electron.* **34**, 451 (2004).
- ¹¹P. G. Schunemann and T. M. Pollak, *J. Cryst. Growth* **174**, 278 (1997).
- ¹²K. J. Range, W. Becker, and A. Weiss, *Z. Naturforsch. B* **23**, 1009 (1968).
- ¹³I. I. Burlakov, Y. Raptis, V. V. Ursaki, and E. Anastassakis, *Solid State Commun.* **101**, 377 (1997).
- ¹⁴V. V. Ursaki, I. I. Burkalov, I. M. Tiginyanu, Y. S. Raptis, E. Anastassakis, and A. Aneda, *Phys. Rev. B* **59**, 257 (1999).
- ¹⁵S. Meenakshi, V. Vijyakumar, B. K. Godwal, A. Eifler, I. Orgzall, S. Tkachev, and H. D. Hochheimer, *J. Phys. Chem. Solids* **67**, 1660 (2006).
- ¹⁶S. Meenakshi, V. Vijyakumar, A. Eifler, and H. D. Hochheimer, *J. Phys. Chem. Solids* **71**, 832 (2010).
- ¹⁷L. Garbato, F. Ledda, and A. Rucci, *Prog. Cryst. Growth Charact.* **15**, 1 (1987).
- ¹⁸I. M. Tiginyanu, N. A. Modovyan, and O. D. Stoika, *Fiz. Tverd. Tela (Leningrad)* **34**, 967 (1992); *Sov. Phys. Solid State* **43**, 527 (1992).
- ¹⁹K. Syassen, *High Press. Res.* **28**, 75 (2008).
- ²⁰G. Kresse *et al.*, computer code VASP; see <http://www.vasp.at>
- ²¹J. P. Perdew, K. Burke, and M. Ernzerhof, *Phys. Rev. Lett.* **78**, 1396 (1997).
- ²²F. J. Manjón, O. Gomis, P. Rodríguez-Hernández, E. Pérez-González, A. Muñoz, D. Errandonea, J. Ruiz-Fuertes, A. Segura, M. Fuentes-Cabrera, I. M. Tiginyanu, and V. V. Ursaki, *Phys. Rev. B* **81**, 195201 (2010).
- ²³O. Gomis, R. Vilaplana, F. J. Manjón, E. Pérez-González, J. López-Solano, P. Rodríguez-Hernández, A. Muñoz, D. Errandonea, J. Ruiz-Fuertes, A. Segura, D. Santamaría-Pérez, I. M. Tiginyanu, and V. V. Ursaki, *J. Appl. Phys.* **111**, 013518 (2012).
- ²⁴A. Eifler, J.-D. Hecht, G. Lippold, V. Riede, W. Grill, G. Krauss, and V. Krämer, *Physica B* **263**, 806 (1999).
- ²⁵A. Eifler, G. Krauss, V. Riede, V. Krämer, and W. Grill, *J. Phys. Chem. Solids* **66**, 2052 (2005).
- ²⁶K. Parlinski, computer code PHONON, see: <http://www.computingformaterials.com/index.html>
- ²⁷S. Baroni, S. Gironcoli, A. del Corso, and P. Giannozzi, *Rev. Mod. Phys.* **73**, 515 (2001).
- ²⁸P. Giannozzi, S. Baroni, P. Bonini *et al.*, *J. Phys.: Condens. Matter* **21**, 395502 (2009).
- ²⁹E. Kroumova, M. I. Aroyo, J. M. Perez-Mato, A. Kirov, C. Capillas, S. Ivantchev, and H. Wondratschek, *Phase Transitions* **76**, 155 (2003).
- ³⁰R. Haeuseler, *J. Solid State Chem.* **26**, 367 (1978).
- ³¹R. Haeuseler, G. Waschenbach, and H. D. Lutz, *Phys. Status Solidi B* **129**, 549 (1985).
- ³²C. Razzetti and P. P. Lottici, *Jpn. J. Appl. Phys.* **32**(Suppl. 32-3), 431 (1993).
- ³³R. Loudon, *Adv. Phys.* **13**, 423 (1964).
- ³⁴P. Alonso-Gutiérrez and M. L. Sanjuán, *Phys. Rev. B* **78**, 045212 (2008).
- ³⁵R. Vilaplana, *et al.*, "Thermally-activated cation ordering in ZnGa₂Se₄ single crystals studied by Raman scattering, optical absorption, and ab initio calculations" (to be published).
- ³⁶D. Errandonea, R. S. Kumar, F. J. Manjón, V. V. Ursaki, and I. M. Tiginyanu, *J. Appl. Phys.* **104**, 063524 (2008).
- ³⁷C. K. Lowe-Ma and T. A. Vanderah, *Acta Crystallogr., Sect. C: Cryst. Struct. Commun.* **47**, 919 (1991).
- ³⁸A. Grzechnik, V. V. Ursaki, K. Syassen, I. Loa, I. M. Tiginyanu, and M. Handfland, *J. Solid State Chem.* **160**, 205 (2001).
- ³⁹M. Cardona, R. K. Kremer, R. Lauck, G. Siegle, A. Muñoz, and A. H. Romero, *Phys. Rev. B* **80**, 195204 (2009).
- ⁴⁰F. Marquez and V. Fornés, *Solid State Commun.* **112**, 17 (1999).